Lab Notes

Editors
Thomas M. Moses | Shane F. McClure

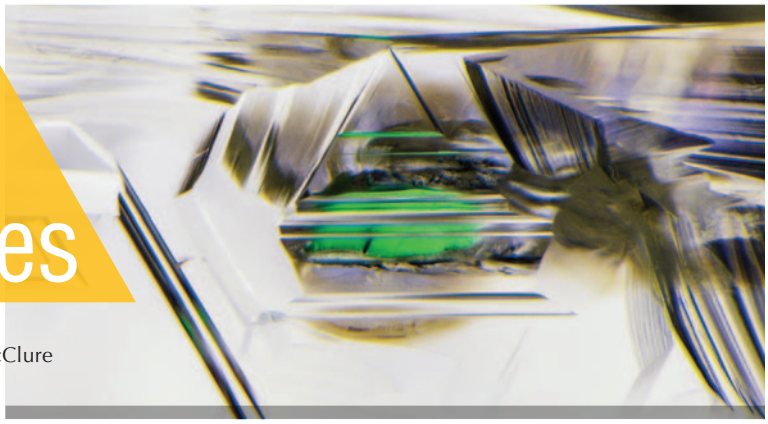

DIAMOND

Asterism in Natural Diamond Cabochons

The New York laboratory received two cabochon diamonds from Hong Kong, both displaying asterism. Gemologists initially questioned whether these stones were in fact diamond because of the cabochon cutting style and the white four-rayed "stars" observed using fiber-optic illumination. The polished cabochon is a popular cutting style in colored stones but rarely attempted with diamond due to its hardness. This cutting and polishing technique yielded two semitransparent to translucent round cabochon diamonds with a very light yellow color, weighing approximately 6.29 ct and 6.07 ct (figure 1).

Mid-infrared spectroscopy revealed strong hydrogen-related absorption bands (e.g., 3107 cm^{-1}) and those attributed to aggregated nitrogen in the one-phonon region, evidence of natural type Ia diamonds (figure 2). Microscopic observation from the base of the cabochons revealed prevalent clouds distributed throughout the diamonds. The clouds were composed of small whitish pinpoints, and when aligned linearly formed small needle-like internal inclusions (figure 3). Fluorescence images collected using the DiamondView revealed yellowish green fluorescence in the sectors with clouds. The cloud-free sectors were inert to UV radiation. Symmetrical fluorescence patterns were observed in both stones with nearly mirror images (figure 4).

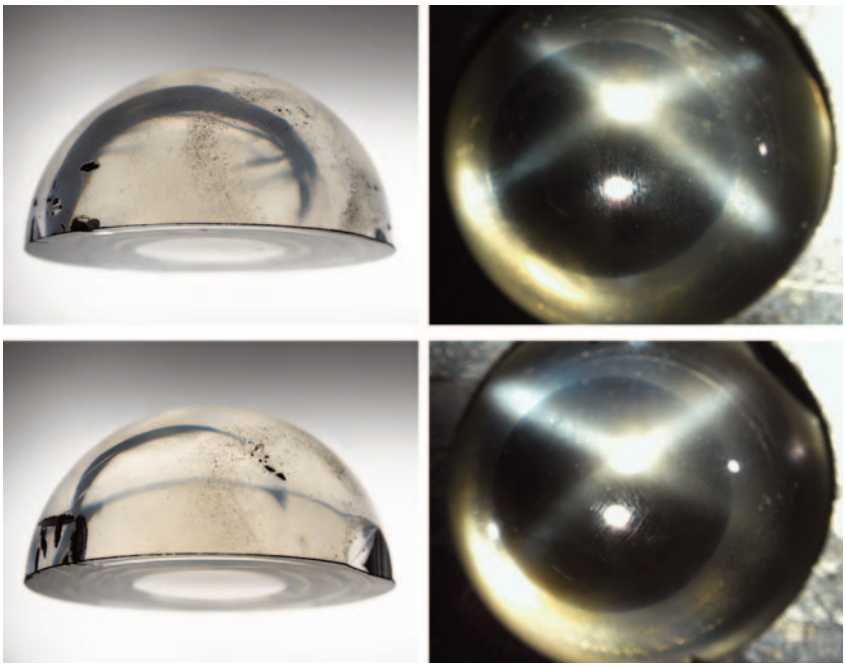

Figure 1. Photos show internal cloud inclusions in profile view (left) and asterism in top view of the polished cabochons using fiber-optic illumination (right). The diameters of the two cabochons are 11.33 mm (top) and 11.32 mm (bottom).

Natural diamonds are dominated by {111} octahedral growth sectors, but occasionally the {100} cubic sector is well developed, forming a crystal with mixed growth habits. The cubic growth sector could preferentially contain a significant amount of pinpoint cloud inclusions. This feature occurs quite often in diamonds from Zimbabwe. Unlike other diamonds with clouds, these clouds concentrated in the {100} growth sectors linearly aligned to form needle-like inclusions. The distribution of these needle-like inclusions within the {100} growth sectors generated the asterism feature seen in these gem diamonds.

Gemological and spectroscopic

Editors' note: All items were written by staff members of GIA laboratories.

Gems & Gemology, Vol. 57, No. 1, pp. 52–62.

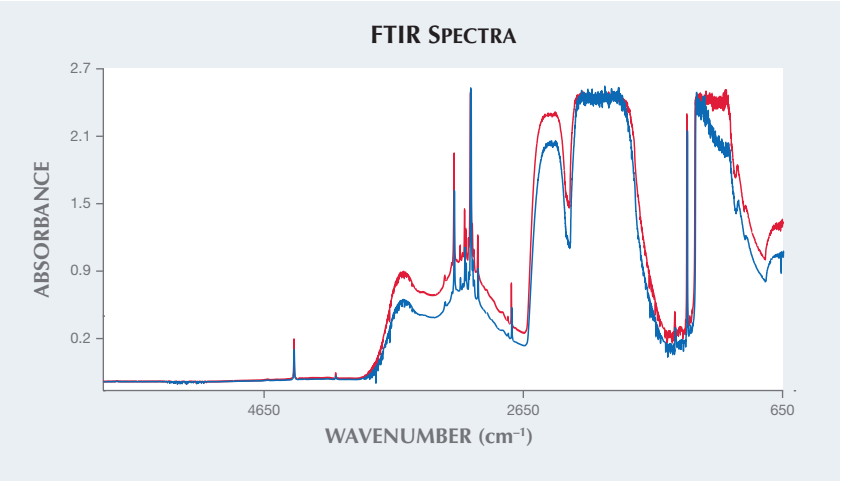

Figure 2. FTIR spectra reveal natural type Ia diamonds with strong hydrogen concentrations in the 3000–4000 cm^{-1} region and aggregated nitrogen in the one-phonon region at 1400–800 cm^{-1}. The 6.29 ct diamond cabochon spectrum is denoted in red and the 6.07 ct diamond in blue.

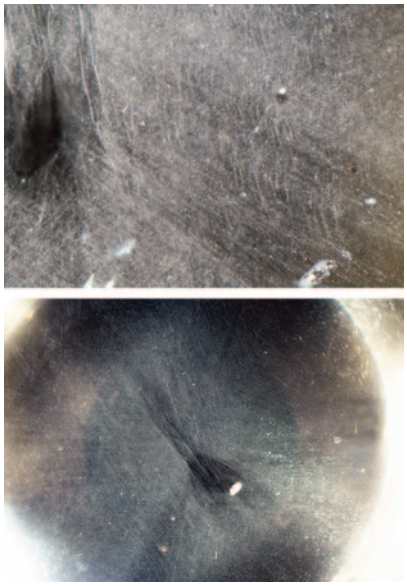

Figure 3. Cloud and needle-like inclusions observed in bottom view of the two very light yellow round cabochon diamonds: 6.29 ct (top, field of view 1.8 mm) and 6.07 ct (bottom, field of view 6.5 mm).

features strongly indicated that these diamonds were cut from the same large rough diamond crystal. The crystal was very likely cut through the center along the (100) plane and then polished into two relatively large cabochon diamonds. Taking advantage of the widespread needle-like inclusions in this otherwise well-included large diamond crystal was a clever design choice to produce two cabochons displaying the rare asterism phenomena.

Erica A. Watts

Bicolor Rough Diamond Crystals

The GIA laboratory in Antwerp regularly receives pink diamond crystals for examination as part of the Diamond Origin Report. This recent service has allowed GIA researchers to study a greater number of rough diamonds in addition to their faceted counterparts. Two crystals, weighing 1.75 and 1.44 ct and both reportedly from Australia, were among those submitted. These were considered quite interesting, as they contained colorless and pink sections with distinct boundaries (figure 5).

The color in the vast majority of naturally pink diamonds is attributed to a broad absorption band at about 550 nm within the visible absorption spectrum. This band generally results from distortion of the crystal lattice from plastic deformation due to stress after crystal growth. However, much remains unknown about the actual formation and configuration of this feature. Therefore, these two crystals provide a unique chance to study natural diamond formation and the origin of pink color in greater detail.

The pink section of both analyzed samples likely experienced great stress in order to undergo the plastic deformation necessary to impart the pink color. The colorless sections were not similarly deformed so presumably they represent a different and later growth event (figure 6).

Visible-NIR absorption spectra collected from the pink and near-colorless sections of the diamonds show differences in the 550 nm region. Observed in the spectrum for the pink

Figure 4. DiamondView images of the very light yellow round cabochon diamonds reveal the location of asterism using ultra-short-wave illumination, approximately 225 nm. The top view is shown on the left in each pair of images, the bottom view on the right.

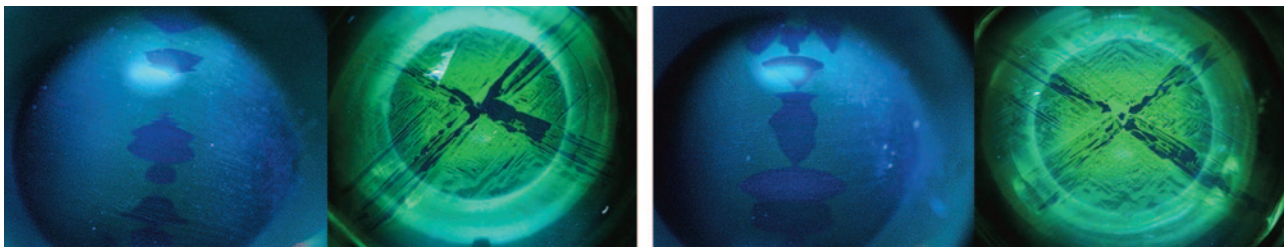

Figure 5. These two rough diamond crystals (1.75 ct on the left and 1.44 ct on the right) are rare examples of diamonds showing both pronounced pink and colorless sections. Field of view 10.8 mm (left) and 7.4 mm (right).

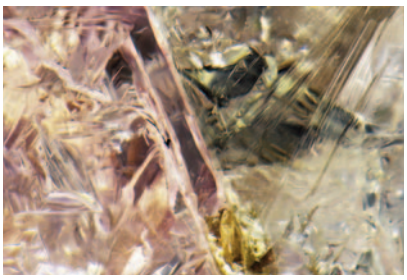

Figure 6. A close-up image of the 1.44 ct diamond crystal shows the boundary between the pink (left) and colorless (right) sections. Field of view 3.16 mm.

portion is the expected absorption at 550 nm, while the spectrum for the colorless portion shows a lack of absorption (figure 7, left).

For the 1.44 ct crystal, we also collected infrared (IR) absorption spectra and photoluminescence (PL) spectra from both the pink and the colorless sections using 455 and 532 nm laser excitation wavelengths. The IR absorption spectra for both sections indicate type Ia diamonds with saturated concentrations of nitrogen. Due to this saturation, it was not possible to determine the total nitrogen content or the ratio of the A and B nitrogen centers, which could have helped in further distinguishing these two sections.

Within the PL spectra, the peak widths for the diamond Raman peak and the H3 peak were comparable in both the pink and colorless sections. Additionally, a PL peak at 676 nm was detected in both sections; although its configuration is unknown, it was documented previously in other rough pink diamonds (E. Gaillou et al., "Spectroscopic and microscopic characterizations of color lamellae in natural pink diamonds," *Diamond and*

Figure 7. Left: Vis-NIR absorption spectra for the 1.44 ct crystal collected from the pink and colorless sections. The 550 nm absorption band is prominently visible within the pink section. The spectra are stacked for clarity. Right: PL spectra with 532 nm excitation of the 1.44 ct crystal show a ~600–730 nm emission band collected from the areas of pink banding, which was not detected from the colorless section—this luminescence band has previously been linked with the 550 nm absorption band. The diamond Raman peaks are scaled as equal.

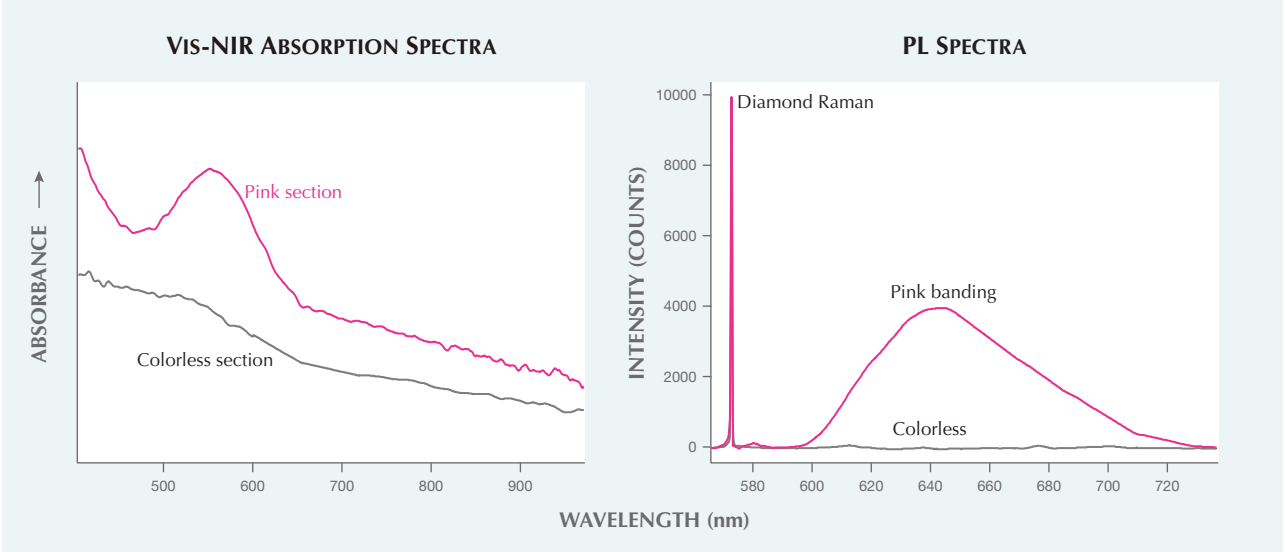

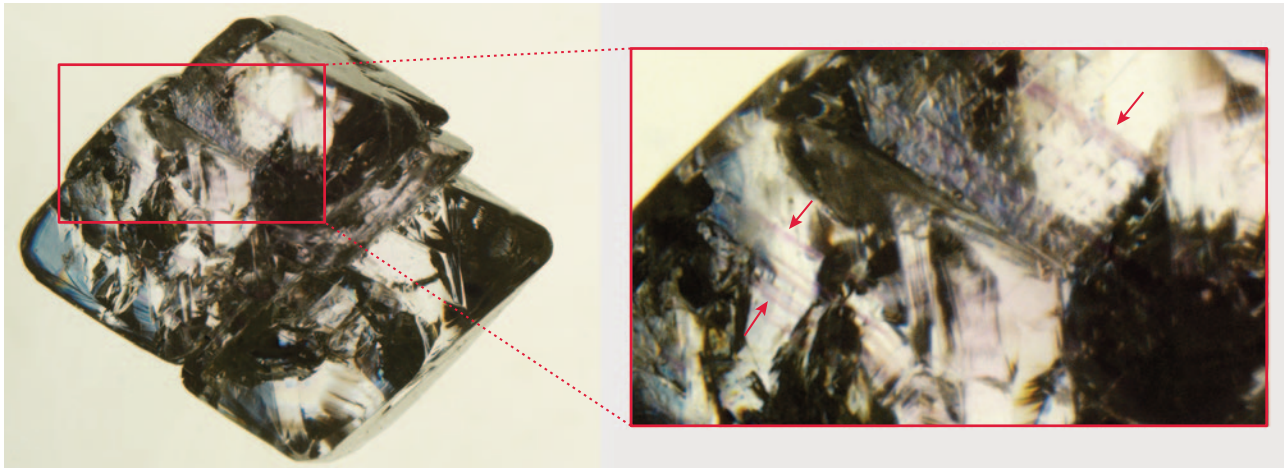

Figure 8. The 1.44 ct crystal was immersed in methylene iodide to reveal additional details. The red arrows within the inset (field of view 3.4 mm) indicate the pink banding.

Related Materials, Vol. 19, No. 10, 2010, pp. 1207–1220). The other notable feature detected by PL mapping was a broad (~600–730 nm) emission band (figure 7, right) that coincided with the pink banding revealed by immersion in methylene iodide (figure 8). Its detection is consistent with other pink diamonds and likely related to the 550 nm absorption band (e.g., S. Eaton-Magaña et al., "Comparison of gemological and spectroscopic features in type IIa and Ia natural pink diamonds," *Diamond and Related Materials*, Vol. 105, 2020, p. 107784).

As natural pink diamonds are quite rare, finding two examples of such bicolor crystals that show these distinct pink and colorless sections is an extraordinary find.

Sally Eaton-Magaña, Paul Johnson, Ellen Barrie, and Michaela Hariňová

Rare Faceted HEXAGONITE

A saturated pinkish purple hexagonite (figure 9) was recently examined at the Carlsbad laboratory. Standard gemological testing revealed a refractive index of 1.599–1.629 and a specific gravity of 2.97 obtained hydrostatically. Microscopic examination showed needle-like inclusions and iridescent cleavage cracks (figure 10). When observed with a dichroscope, pleochroic colors of pink,

Figure 9. This 3.27 ct pinkish purple hexagonite is the largest example examined by the authors. Courtesy of Vance Gems.

Figure 10. Iridescent cleavage cracks and needle-like structures were present in the faceted hexagonite. Field of view 3.50 mm.

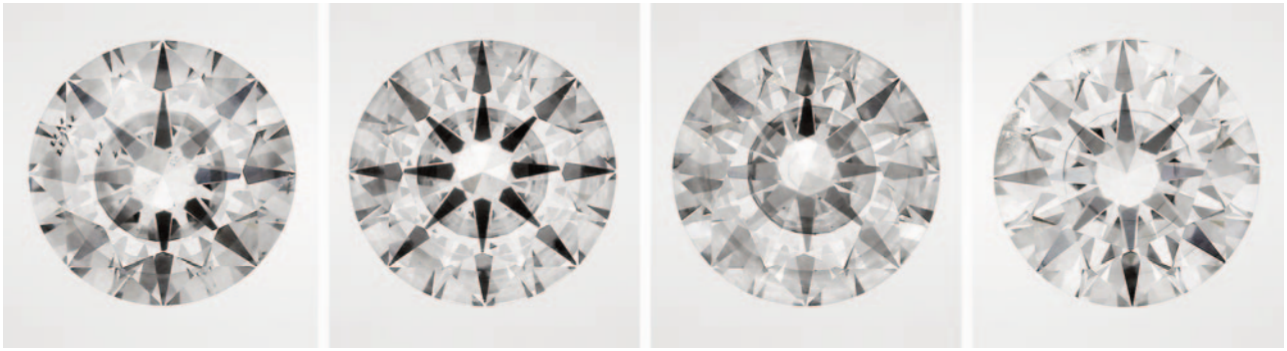

Figure 11. Face-up images of four CVD laboratory-grown diamonds with an eye-visible growth plane. These four diamonds range from 1.81 to 2.51 ct.

orangy pink, and violet were observed. These results were consistent with the mineral tremolite. The pinkish purple variety of tremolite is recognized as hexagonite, which owes its color to manganese. Hexagonite was once thought to be a hexagonal form of tremolite, which is how its name was derived, but was later confirmed to be monoclinic (Summer 1985 Gem News International, p. 110).

This particular stone was faceted by Bill Vance of Vance Gems, who sourced the rough that was reportedly from the original type locality, the Balmat-Edwards zinc mining district in St. Lawrence County, New York. Hexagonite is also found at the town of Fowler in St. Lawrence County. The saturated pinkish purple color and large size make this rare stone an exceptional example of this material. While very few faceted hexagonite gems have been tested at GIA, this 3.27 ct stone is the largest one examined by the authors.

Amy Cooper and Nathan Renfro

Prominent Growth Planes Observed in HPHT-Processed CVD LABORATORY-GROWN DIAMONDS

The laboratory-grown diamond industry is ever evolving and improving. With state-of-the-art growth and treatment technology, high-quality CVD diamonds, in terms of clarity and color, are now commonly seen on the consumer market. Laboratory-grown diamonds are occasionally submitted for natural diamond grading services, and recently GIA's Hong Kong laboratory received a total of 43 undisclosed CVD-grown diamonds treated by high pressure and high temperature (HPHT), ranging from 0.70 to 2.63 ct in weight, from the same client. Laboratory-Grown Diamond Reports were issued for these synthetics, which received E–I color grades and VVS_2–I_2 clarity grades.

Four samples had a very eye-catching feature—a dark circle or ring at the center when viewed face-up without magnification. The ring appeared to be a thick grayish layer at the culet when viewed from the pavilion (figure 11). As the extraordinary feature looked shiny and resembled the separation plane often observed in assembled stones, questions about the true identity of these samples were raised.

Figure 12. Visible planes with different textures: fine clouds (top left, field of view 3.83 mm) and wave ripples (top right, field of view approximately 3 mm). Colorless "holes" observed in a ripple-like plane under the microscope (bottom left, field of view 3.83 mm) and in immersion (bottom right). The blue color in the top left photo is due to a different white balance to emphasize the texture.

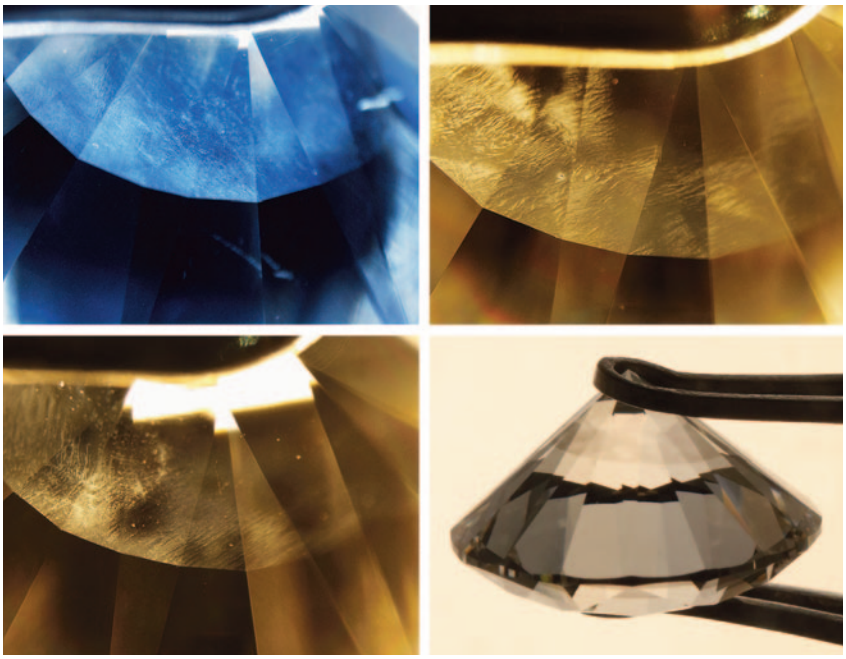

Microscopic examination of these four samples revealed some interesting findings. There was a textured plane almost parallel to the table facet, each with a different appearance (figure 12): fine clouds all the way across; ripple-like waves with some "holes" (colorless areas); a mixture of both; and a ripple-like plane that was not visible all the way around. An additional 26 samples had visible grayish/brownish planes either at the pavilion, which were much less prominent, or at the pavilion viewing through the table. Eight of these additional samples had a plane at an angle to the table facet. The plane appeared as a line with no color difference when immersed in water and viewed in a parallel direction to the growth plane. All 43 samples generally showed a banded and cross-hatched strain pattern when viewed with crossed polarizers (figure 13).

Spectroscopic analysis of the 43 samples yielded very similar results. They were either type IIa or type IIb and had a very strong silicon vacancy doublet peak (736.5 and 736.9 nm) in their photoluminescence spectra, typical of CVD-grown diamonds. PL spectra were also collected at the table and at the pavilion somewhere between the growth plane and the culet for the samples with a very prominent growth plane, but the data did not show any critical differences. The most diagnostic test was DiamondView imaging, as all 43 displayed very distinct growth layers (figure 14). It also revealed the HPHT treatment history that the CVD diamonds had experienced.

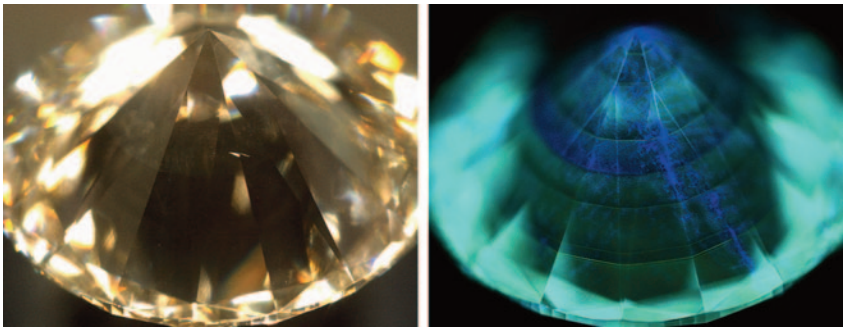

Figure 14. DiamondView imaging provided evidence of CVD growth.

The uniformity of the growth layers observed in DiamondView imaging and under crossed polarizers, together with the immersion test, showed no evidence of assembly and therefore excluded the possibility of a doublet. The color making the growth plane visible is believed to come from the non-diamond carbon deposited between two growths. It could not be removed by the post-growth HPHT treatment.

Billie Pui Lai Law, Ka Wing Tam, and Nick Ka Chun Chan

OPAL

Cat's-Eye Opal

Precious opal characteristically shows a spectacular play-of-color effect and may also display cat's-eye or star phenomena produced by the internal structure (e.g., Winter 1990 Gem News, p. 304; Spring 2003 Lab Notes, pp. 43–44; Summer 2014 Lab Notes, pp. 152–153). Chatoyancy and asterism in opal are quite rare, however, because opal is a hydrated silica and has no repeating crystal lattice (J.V. Sanders, "The structure of star opals," *Acta Crystallographica*, Vol. A32, 1976, pp. 334–338). The keys to creating and maximizing chatoyancy in opal is careful arrangement of the play-of-color patches, orienting the "brushstrokes" (stripe structure caused by misalignment of the tiny silica spheres producing play-of-color), and good cutting.

Recently, GIA's Tokyo laboratory had an opportunity to examine a transparent double cabochon measuring 12.65 × 10.06 × 5.70 mm and weighing 3.79 ct. It showed blue to green play-of-color against a gray background as well as a distinct chatoyancy (figure 15). Standard gemological testing gave a specific gravity of 2.13

Figure 13. A banded strain pattern seen across the visible plane. Field of view 11.45 mm.

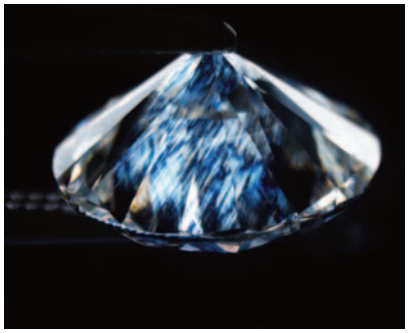

Figure 15. This 3.79 ct gray transparent opal shows dominant blue play-of-color with a distinct chatoyancy.

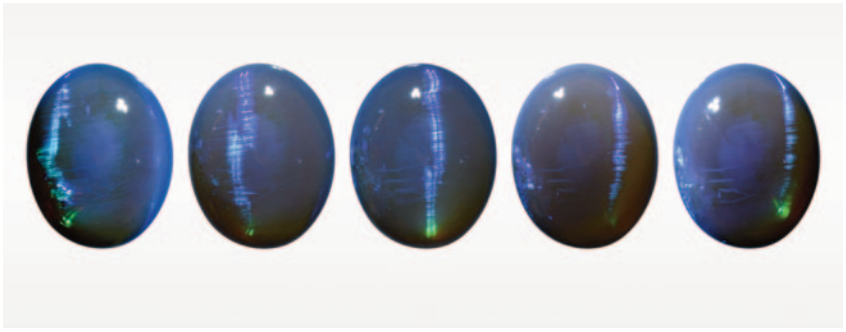

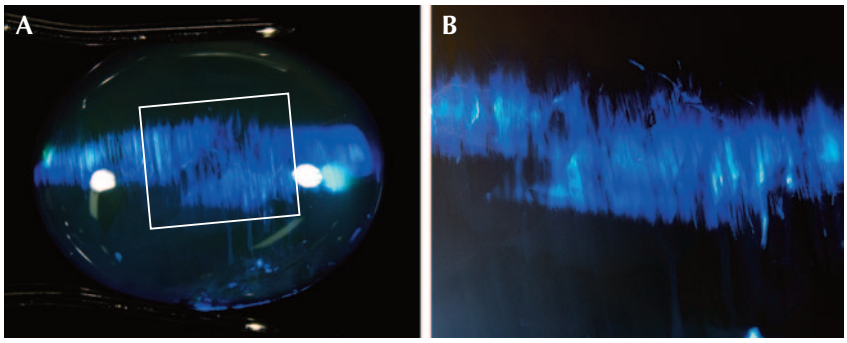

Figure 16. Chatoyant effect caused by light reflecting off parallel brushstroke patterns within play-of-color patches. A: This opal contained several large play-of-color patches with parallel brushstrokes. B: A close-up of the brushstroke pattern seen in the white square in (A). Field of view 13.3 mm (A) and 5.60 mm (B).

and a spot RI reading at 1.45, suggesting that the stone was opal. The brushstroke pattern within play-of-color patches and the strong bluish white fluorescence and phosphorescence after exposure to ultraviolet light were consistent with a natural origin. Advanced testing using Fourier-transform infrared spectroscopy (FTIR) also indicated that this was natural opal with no evidence of polymer impregnation and/or sugar treatment (G. Brown, "Treated Andamooka matrix opal," Summer 1991 *G&G*, pp. 100–106). This opal had no synthetic features such as "snake skin" and "columnar structure" in any direction. There was no evidence that this stone was assembled.

In microscopic observation, this opal contained several large blue to green play-of-color patches with parallel brushstroke patterns. The brushstrokes in each patch were mostly perpendicular to the length of the stone and parallel to each other, and the light reflection from the pattern created a distinct chatoyant effect (figure 16). Because the opal was composed of large blue dominant play-of-color patches, the parallel brushstrokes and the high-dome cabochon shape produced a distinct chatoyancy against the gray background. This was a striking example of cat's-eye precious opal.

Makoto Miura and Yusuke Katsurada

Figure 17. Opal with unusual aventurescence, seen with fiber-optic lighting.

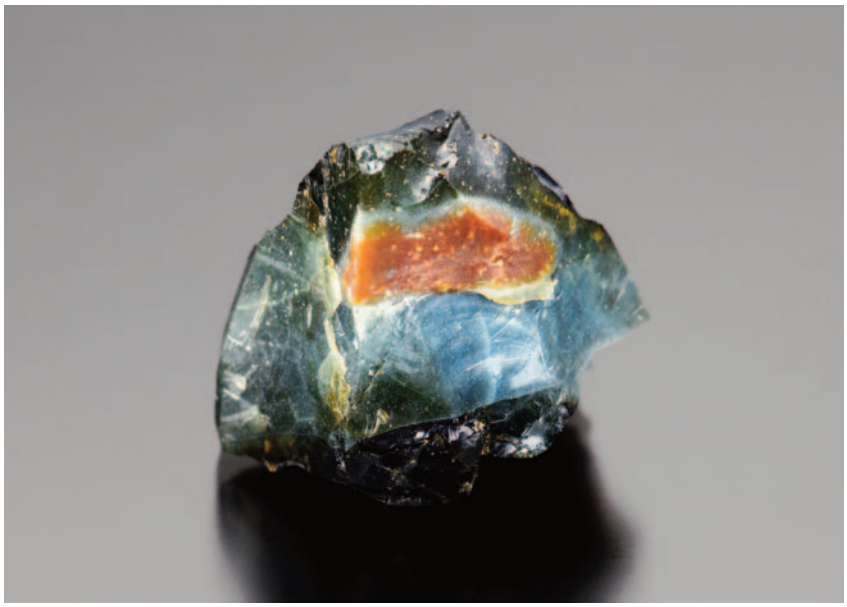

Green Opal Displaying Aventurescence

Recently the Carlsbad laboratory received a variegated dark green and blue partially polished rough stone for identification services. The stone measured 23.64 × 20.13 × 15.52 mm and weighed 23.74 ct (figure 17). A vitreous to waxy luster and bright yellow inclusions were observed.

Standard gemological testing revealed a refractive index spot reading of 1.43 and a specific gravity of 2.15 obtained hydrostatically. These properties were consistent with opal. During microscopic analysis, fine hazy clouds and turbidity were seen within the structure, as well as a reddish brown portion with iron staining. Although no play-of-color was observed, an unusual aventurescence was seen in several areas with fiber-optic lighting while rotating the stone. This unusual phenomenon was caused by the scattering of light from the small, eye-visible yellow inclusions (figure 18). These inclusions were later confirmed by Raman spectroscopy as pyrite.

Figure 18. Scattered inclusions in the green opal were identified by Raman spectroscopy as pyrite. Field of view 1.79 mm.

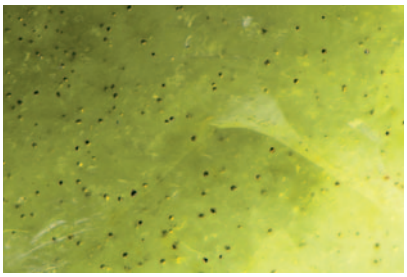

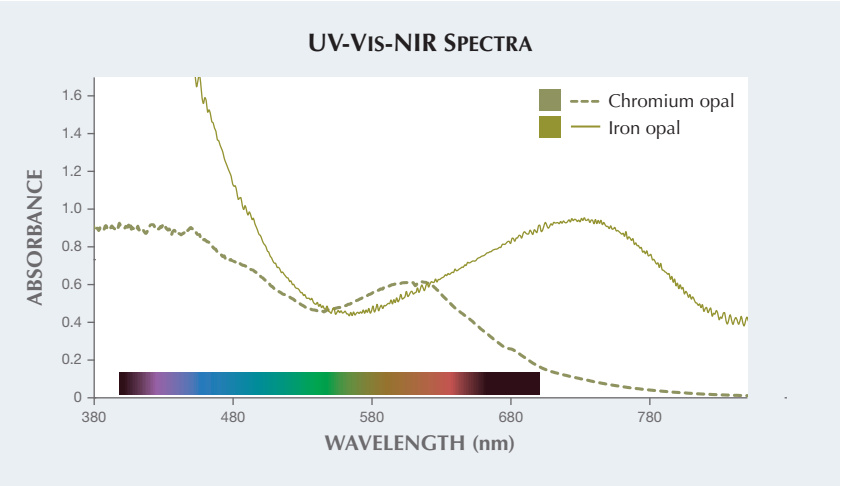

Figure 19. The spectra of the two types of opal were measured and renormalized for comparison with each other with similar lightness (see corresponding color panels in table 1). The solid line represents iron opal. The broad absorption band centered at 741 nm is likely caused by interstitial Fe^{2+}. The dashed line represents chromium opal. The smaller absorption band centered at around 600 nm is caused mainly by Cr^{3+}.

LA-ICP-MS analysis was performed on the sample to investigate which chromophore was responsible for its green color. The results showed that the stone contained approximately 3540 ppma Fe. No other chromophoric trace elements were measured in significant quantities, indicating that iron was most likely the cause of the green color. UV-Vis-NIR spectra were collected and used to quantitatively calculate the color of this material (figures 19 and 20, table 1). In figure 19, a broad absorption band centered at about 741 nm produces the green color of the opal. This absorption band is likely related to octahedral Fe^{2+}. Previous publications have shown that iron can produce green color in quartz due to an absorption band centered at 741 nm relating to interstitial Fe^{2+} (L.B. Hebert and G.R. Rossman, "Greenish quartz from the Thunder Bay amethyst mine panorama (TBAMP), Thunder Bay, Ontario, Canada," *Canadian Mineralogist*, Vol. 46, No. 1, 2008, pp. 111–124). Octahedral Fe^{2+} can strongly absorb red, orange, and some portion of yellow light of the visible spectrum to produce a transmission window in the yellowish green region. In this case, a transmission window around 570 nm results in the green color in the iron opal (solid line in figure 19). The presence of some additional Fe^{3+} cannot be ruled out and may contribute to the rise in absorption at shorter wavelengths into the UV region.

Another type of green opal colored by Cr^{3+} (Winter 2020 Lab Notes, pp. 520–521) was compared with the iron-colored opal (solid line in figure 19). Cr^{3+} produces a smaller absorption band centered at about 600 nm, leading to a transmission window in the green region around 540 nm that causes a less yellow and more pure green color (figure 19). The two color panels calculated from the two spec-

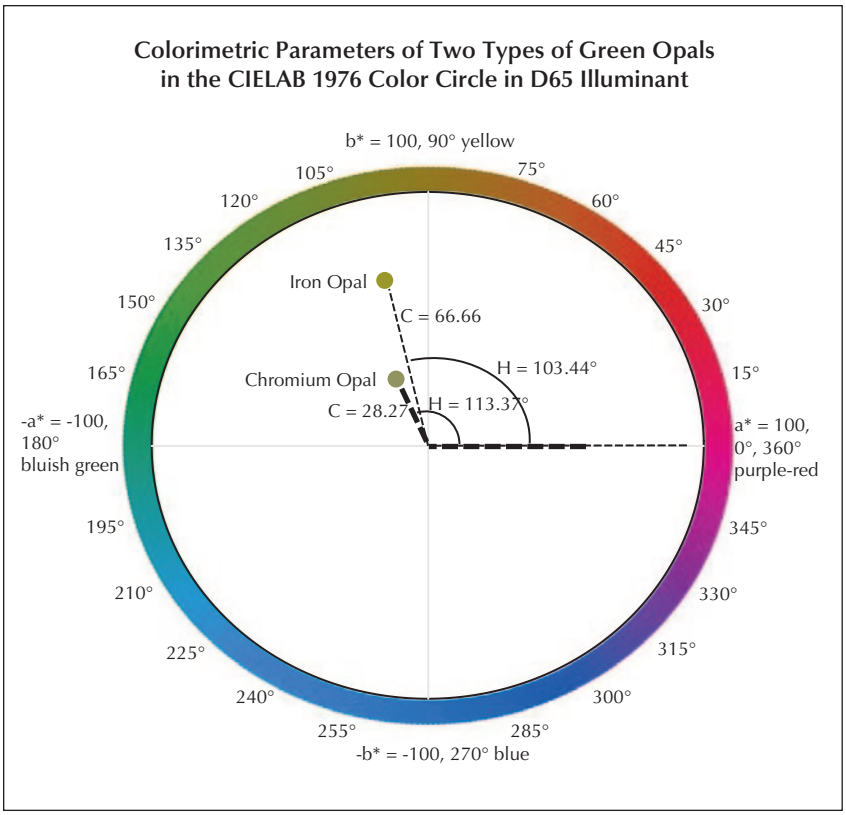

*Figure 20. Color panels corresponding to the two spectra were plotted in the CIE L*a*b* 1976 color circle. The color of the iron opal, looking more yellowish and saturated, has a smaller hue angle and larger chroma than the color of the more greenish and less saturated chromium opal. Both calculated color panels have similar lightness for comparison (table 1).*

TABLE 1. CIE and RGB color coordinates calculated from the two opal spectra in figure 19 under CIE D65 illumination.

Iron opal				Chromium opal			
D65	L*	a*	b*	D65	L*	a*	b*
	60.17	-15.49	64.84		60.90	-11.21	25.95
	L	C	H		L	C	H
	60.17	66.66	103.44		60.90	28.27	113.37
	X	Y	Z		X	Y	Z
	0.23	0.28	0.04		0.25	0.29	0.17
	R	G	B		R	G	B
	148.68	150.50	0.00		144.05	151.41	100.55

tra were also plotted in the CIE L*a*b* 1976 color circle seen in figure 20. This allows for a more accurate comparison between the two color panels using quantitative colorimetric data. In the plot, the hue angle of the iron opal is smaller than chromium opal, resulting in a more yellowish green hue. The chroma of the iron opal is larger than that of a chromium opal with similar lightness, resulting in a more saturated color.

This green common opal is a clear example of iron contributing to the yellowish green color, in contrast to the more pure green color due to the chromium in the opal previously documented with a slightly grayish green color. Both the yellowish green color and pyrite inclusions are consistent with an iron-rich environment. The pyrite inclusions also add a unique display of aventurescence not typically seen in common opal.

Amy Cooper, Ziyin Sun, Philip York, and Aaron Palke

Natural Fossil PEARLS and Shell Blister from the Coast of Florida

Fossilized shells and pearls represent a unique group of specimens that are occasionally submitted to GIA, as reported in *G&G* previously (Winter 2015 Lab Notes, pp. 432–434; Spring 2020 Lab Notes, pp. 136–138). Those fossil samples were usually brownish in color and fully petrified, lacking any surface structures and associated luster or overtones that once belonged to them. However, two cream-colored fossil pearls (along with a fossil shell containing a shell blister; figure 21) recently submitted to GIA's New York laboratory completely changed our earlier impressions.

The two semi-baroque-shaped pearls measuring approximately 12.64 × 11.50 × 10.00 mm (weighing 8.64 ct) and 13.08 × 11.45 × 10.18 mm (weighing 9.48 ct) exhibited a dry, chalky appearance that would be expected for such old samples, with cracks and parasite holes (figure 22, right) detectable by visual observation. More remarkably, some surface areas had delicate nacre layers showing fine nacre platelet structures and displaying subtle iridescence effect, which could be considered as orient in nacreous pearls (figure 22). EDXRF analysis detected low concentrations of manganese and high concentrations of strontium, typical for marine mollusks. Raman spectroscopy identified the composition of the materials as aragonite. Microradiography revealed internal concentric and arc growth features, which confirmed their natural origin. Out of curiosity and due to the very good condition of the two pearls, we

Figure 21. Three fossilized specimens recently submitted to GIA's New York laboratory: two fossil pearls (12.64 × 11.50 × 10.00 mm and 13.08 × 11.45 × 10.18 mm, left and right, respectively) and a fossil shell (45.97 × 32.03 × 10.90 mm) containing a shell blister. Courtesy of Kathryn Malatino and Aaron Brown.

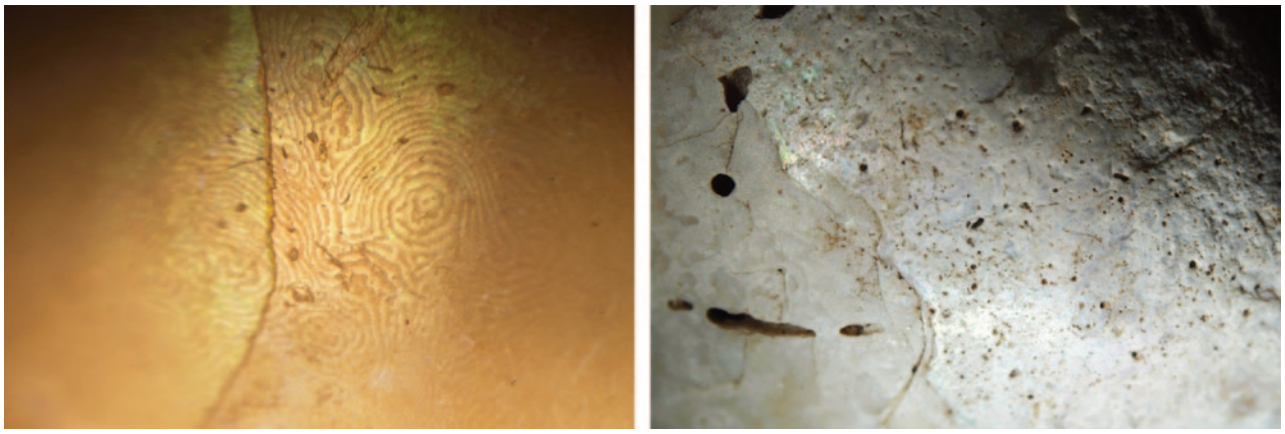

Figure 22. Nacreous spiral platy structures, parasite tunnels, and orient effects were observed on the surfaces of the two fossil pearls. Field of view 1.5 mm (left) and 5.9 mm (right).

further extracted a small amount of powder from the surface of one pearl and sent it to the Accelerator Mass Spectrometry Lab at the University of Arizona for radiocarbon dating analysis. The dating work resulted in a $\delta^{13}C$ value of –0.8 ‰, proving the sample to be very old. The fraction of modern carbon is less than 0.0024, indicating that the age of the sample was beyond the limit of radiocarbon dating (>48,500 years), though the actual age is unknown. This result proved that the sample could be categorized as fossilized material.

The shell that was submitted along with the two fossil pearls looked more petrified but also remained relatively intact, with obvious ridges (or scutes) on the back of the shell and a shallow cream-colored "bump" on the inner side that could best be described as a shell blister. According to the owner, these fascinating specimens were found off of the west coast of Florida near St. Petersburg, approximately 25–50 feet below the sediment during dredging, along with many more shells of various kinds and even fossilized shark teeth.

The two natural fossil pearls and the shell blister created by Mother Nature have been well preserved. They provided unique insights into ancient mollusks and their associated pearls or related materials.

Chunhui Zhou

Lead Glass–Filled LABORATORY-GROWN RUBY

The GIA lab in Carlsbad received for identification a lead glass–filled laboratory-grown ruby (figure 23). We commonly see glass-filled natural rubies, but to our knowledge only one other laboratory-grown example has ever been submitted.

This transparent to semi-transparent oval mixed cut weighed 3.53 ct and showed gemological properties of ruby: a refractive index of 1.761–1.769, a birefringence of 0.008, a specific gravity of 4.01, a uniaxial optic figure, and a characteristic ruby spectrum using a handheld spectroscope.

Examination of the stone under magnification showed a network of interconnected fractures. A pronounced blue and orange flash effect was observed throughout, proving the fractures were filled with lead glass. Also present in the fractures were dendritic patterns and coarse flattened gas bubbles (figure 24). No inclusions

Figure 23. This 3.53 ct laboratory-grown ruby was treated with lead-glass filling.

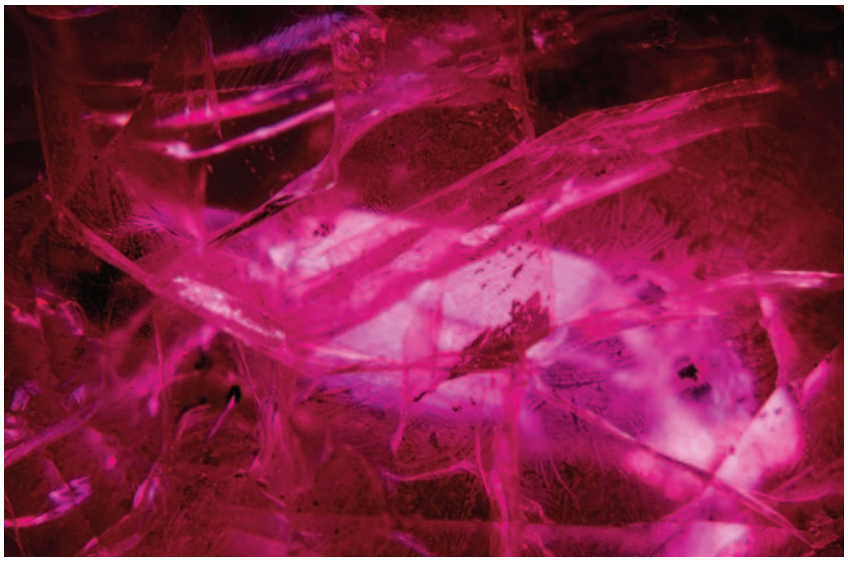

Figure 24. Magnification of the internal structure of the synthetic ruby; both high-relief trapped gas bubbles and blue and orange flash effects were observed in the stone. Field of view 7.19 mm.

were observed to indicate the natural or synthetic origin of the corundum. However, this stone exhibited strong red fluorescence to long-wave ultraviolet and medium chalky (bluish white) red short-wave ultraviolet fluorescence. Chalky SWUV is typical of heated ruby and sapphire. But when viewed in synthetic pink sapphire and synthetic ruby, it generally makes it more difficult to observe diagnostic curved striae in the stone. In our sample it was much harder, since that effect was combined with interference from filled fractures.

In these cases, a stronger SWUV light source may prove helpful. The curved growth lines were seen as chalky luminescent bands in the DiamondView, proof of its laboratory-grown origin (figure 25).

Lead-glass filling of corundum is based on the same principle applied to emerald and diamond: the use of a filling material with an RI very close to that of the host material, to minimize the appearance of fractures. The treatment is very effective, and the clarity of very low-quality material can be improved, rendering it usable in jewelry. This makes it possible to market a great deal of previously unsalable material. Fortunately, this treatment is easily detected with magnification. The identifying characteristics are very low-relief fractures, flattened and rounded gas bubbles and voids (unfilled areas) in fractures, and a blue and orange flash effect (S.F. McClure et al., "Identification and durability of lead glass–filled rubies," Spring 2006 *G&G*, pp. 22–33). This stone displayed an orange and blue flash effect (again, see figure 24) as well as gas bubbles trapped in fractures that were conclusive evidence for lead-glass filling of the fractures in this synthetic ruby. While it is unclear why anyone would go to the trouble to treat a synthetic ruby with lead-glass filling, gemologists should be aware that such material does exist in the trade.

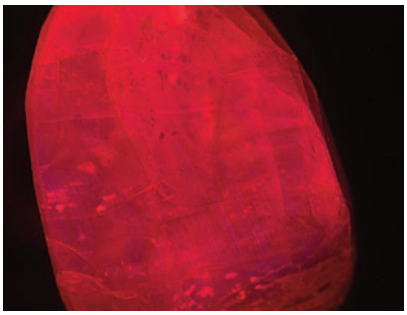

Figure 25. Curved growth striations were observed in the stone using the DiamondView, conclusively proving the synthetic origin of this ruby.

Forozan Zandi

PHOTO CREDITS
Christopher Vendrell—1, 3, 4; Kyaw Soe Moe—4; Michaela Hariňová—5 (left); Nathan Renfro—5 (right), 6, 10, 18; Troy Ardon—8; Robert Weldon—9; Johnny Leung—11, 12 (bottom right); Tony Leung—11; Billie Law—12, 13, 14; Shunsuke Nagai—15; Makoto Miura—16; Diego Sanchez—17, 23, 24; Sood Oil (Judy) Chia—21; Joyce Wing Yan Ho—22 (left); Emiko Yazawa—22 (right); Forozan Zandi—25